Open Archive TOULOUSE Archive Ouverte (OATAO)

OATAO is an open access repository that collects the work of Toulouse researchers and makes it freely available over the web where possible.

Any correspondance concerning this service should be sent to the repository administrator: staff-oatao@inp-toulouse.fr.

Influence of hydrogen bonds on glass transition and dielectric relaxations of cellulose

Frédéric Roig, Eric Dantras, Jany Dandurand and Colette Lacabanne

Physique des Polymères, Institut Carnot CIRIMAT UMR 5085, Université Paul Sabatier 118, route de Narbonne, 31062 Toulouse Cedex, France

E-mail: dantras@cict.fr

Abstract

The molecular dynamics in hydrated cellulose has been investigated by a combination of thermal analyses and dielectric spectroscopy. Differential scanning calorimetry shows the dependence upon hydration of the glass transition temperature T_g. A physical ageing phenomenon has been observed. At the molecular scale, bound water is hydrogen bonded to polar sites of cellulose macromolecules. At the macroscopic scale, water molecules play the role of a plasticizer for cellulose lowering its T_g. Dynamic dielectric spectroscopy combined with thermostimulated currents have allowed us to follow more localized molecular mobility. The β relaxation mode is characterized by activation entropies that vanish for higher water contents indicating molecular mobility localization. It is plasticized by water like the glass transition. This analogy is explained by a common origin of both mechanisms: the mobility of the cellulose backbone. The evolution of the γ mode upon hydration follows an anti-compensation law. Water acts as an anti-plasticizer in a hydrogen bonded network.

1. Introduction

Cellulose is probably the most studied biopolymer. Increasing CO_2 stimulates photosynthesis of chlorophyll plants and potentially allows plants to increase production biomass in the order of 20% [1]. The major structural component of the plant cell and the most important substance produced by plants is cellulose [2]. The large number of studies published on its properties is explained by important interests to optimize the natural resource consumption [3, 4], prevention of fire [5], bone regeneration [6], specific cellulose membranes [7, 8] or decrease the cost of cellulose extraction process by wood genetic modification [9] in the paper industry for example.

Thermal stability has been characterized by thermogravimetry analysis (TGA) [10] and physical structure by differential scanning calorimetry (DSC) [11]. In the literature, thermogravimetry analyses of cellulose point out two weight losses; the first one in the range 40–80 °C attributed to the water evaporation [11–13], and the second one in the temperature range 200–400 °C, to polymer degradation. During this decomposition, the principal products are water and carbon dioxide [5, 11, 12, 14, 15].

The glass transition of cellulose has been extensively studied [11, 16–18], generally by DSC [19]. The determination of the glass transition temperature is not easy due to the presence of water [16] and to the weak fraction of amorphous phase [20]. A similar problem has already been noted for starch-based materials and various factors such as sample preparation, methods of adding water, effect of sample mass or heating rate influence have to be carefully considered [21]. According to Hatakeyama [20], physico-chemical properties of cellulose are mainly dependent upon amorphous regions. By x-ray diffractometry (XRD) the amorphous content of various kinds of cellulose is measured. It reaches 30% for natural cellulose extracted from cotton linter [20]. Batzer and Kreibich [16] determine T_g by DSC but they have small changes in heat capacity. Szczesniak and Rachocki [11] also have small variations in heat capacity. Vittadini *et al* [17] do not observe T_g but molecular transition is found by nuclear magnetic resonance (NMR).

Dynamic dielectric spectroscopy (DDS) has already been used on polysaccharides such as cellulose and its derivatives [22–29]. Four dielectric relaxation modes are usually observed γ, β, β_{wet} and α in the order of increasing temperatures

[22–29]. The dielectric properties of cellulose have also been investigated by combined DDS/thermostimulated current (TSC) [28]. In the low temperature range ($T < 0\,°C$) where the molecular mobility is localized, two modes are extracted; i.e. γ and β also observed in mechanical spectroscopy [30, 31]. The γ mode has been associated with side groups (–CH$_2$OH and –OH) mobility [22–28] and the β mode with localized cooperative molecular mobility of the main chain [28, 29]. The β_{wet} relaxation mode is observable at room temperature and is not detected after intense drying. This mode is attributed by Einfeldt *et al* [22–27] to the reorientation of polymer–water complexes formed at the polymer–water interface. At a higher temperature ($T > 0\,°C$) the molecular mobility is delocalized. α relaxation mode is assigned to cooperative delocalized mobility of nanometric sequences of the main chain [28]. It is the dielectric manifestation of glass transition.

According to Einfeldt *et al*, the properties of polysaccharides such as cellulose can be changed drastically by adding small amounts of water. Moreover, the ability of cellulose to interact with water is not reversible, after consecutive dryings the water retention value of cellulose decreases drastically. This phenomenon is known as hornification [22, 23, 26]. The influence of hydration on relaxation modes of polysaccharides is noticeable. Einfeldt compares dry and wet celluloses. The activation energy E_{a} of the local main chain dynamics increases in contrast to the pre-exponential factor τ_0 which is reduced. The γ process is more cooperative in wet celluloses than in dry celluloses [25]. Measurements on others polysaccharides such as starch and dextran confirm these results [22]. A β_{wet} relaxation mode can be observed in all wet polysaccharides in the room temperature range (0–60 °C) [22–27]. This mode is not observed anymore after drying the sample [22–27]. The hydration influence of polysaccharides on their dielectric properties can be interpreted by several hypotheses: one the one hand, the OH-groups of glucosidic units form hydrogen bonds with water molecules. These bound water molecules increase the dipolar moment and the moment of inertia of movable groups. Moreover, the stiffness of the polymer chain increases because water molecules bonded produce a bridge along the chain and between two adjacent chains. On the other hand, the macroscopic flexibility of a cellulosic fibrous sample becomes more important thanks to the swelling power of water [2, 22, 25].

In spite of the abundant literature, some points such as the complex interaction of water with cellulose macromolecule remain particularly obscure and multiple interpretations exist [32–34]. We have already shown that the fruitful synergy of DDS/TSC combination allows us to investigate the changes within the molecular dynamics of cellulose caused by water influences [28, 29]. These results stimulate us to study the issue of cellulose glass transition with different water contents using the classical techniques of DSC. A complete dielectric study will be performed and particular attention will be paid to specific interactions between polymer and water.

2. Experimental

2.1. Materials

The cellulose provided by Sigma–Aldrich is a white microcrystalline powder (20 μm) extracted from cotton linters, with a number-average molecular weight between 36000 and 40000. The degree of polymerization is between 222 and 246. The initial water content has been determined by thermogravimetry experiments near 5%. Cotton fibres extracted from a natural plant have also been investigated (purity 95%).

Samples with different hydration levels were prepared. The 0% hydration was obtained according to the following procedure: the sample was placed on P$_2$O$_5$ for 72 h. Constant humidity level was reached by storage at 25 °C over saturated salt solutions for 72 h. Saturated salt solutions of MgCl$_2$, 6H$_2$O and NaCl allow us to obtain 3% and 7% of hydration, respectively. In the case of NaCl solution, for a double storage time, 13% was reached.

The water content was determined from the weight loss after drying. The hydration level $h(\%)$ was defined as follows:

$$h(\%) = \frac{m_{\text{water}}}{m_{\text{cellulose}}} \times 100 \qquad (1)$$

where m_{water} is the water mass and $m_{\text{cellulose}}$ is the mass of cellulose sample after drying.

2.2. Methods

2.2.1. Thermogravimetry.
Thermogravimetry analyses were performed with a TGA Q50 thermal analyser in open pans under nitrogen flow from room temperature to 600 °C at 10 °C min^{-1}. Sampling of cellulose was twofold: powder or pellets. Activation energy of cellulose degradation is analysed using the Broido method [35]:

$$\ln(-\ln(1 - \alpha)) = \ln(K) - \frac{\Delta E}{RT} \qquad (2)$$

$$\alpha = \frac{m_0 - m}{m_0 - m_\infty} \qquad (3)$$

where m_0 is the initial mass and m_∞ is the final mass of the sample.

2.2.2. Standard DSC.
The DSC thermograms were recorded with a DSC 2920 TA instrument. The samples in pellets gave better results than powder (associated with signal-to-noise ratio). Cellulose powder was pressed under controlled pressure of about 75 MPa to form pellets. Samples were sealed into aluminium pans, and empty pans were used as reference. Empty pans were also sealed. Experiments were performed in the −20 to 180 °C temperature range with a heating rate 20 °C min^{-1} (and a cooling rate $q_{\text{c}} = 20\,°C\,\text{min}^{-1}$). This heating rate has been chosen to perform the thermal signal [36].

2.2.3. Dynamic dielectric spectroscopy.

A BDS 4000 Novocontrol broadband dielectric spectrometer system was used to obtain the dielectric relaxation map in a wide temperature and frequency range. The sample was inserted between two plan parallel electrodes. It was stimulated by a sinusoidal electrical field at a given temperature and the complex impedance is recorded during frequency scan. The measurements were carried out in the frequency range 10^{-1}–10^6 Hz from -150 to $200\,°C$ by steps of $5\,°C$. The complex dielectric permittivity $\varepsilon^*(\omega)$ was deduced thanks to complex impedance by the relation:

$$\varepsilon^*(\omega) = \frac{1}{\mathrm{i}\omega \cdot C_0 Z^*(\omega)} = \varepsilon' - \mathrm{i}\varepsilon'' \tag{4}$$

with C_0 the capacitance in vacuum, ω the pulsation ($\omega = 2\pi f$), Z^* the complex impedance. Relaxation modes are described by the Havriliak–Negami (HN) function [37]:

$$\varepsilon^*(\omega) = \varepsilon_\infty + \frac{\Delta\varepsilon}{[1 + (\mathrm{i}\omega\tau_{HN})^{\alpha_{HN}}]^{\beta_{HN}}} \tag{5}$$

with τ_{HN} the relaxation time of the HN equation, α_{HN} is the width and β_{HN} the asymmetry of the mode.

In cellulose, the temperature dependence of relaxation times follows an Arrhenius–Eyring equation:

$$\tau(T) = \frac{h}{k_B \cdot T} \cdot \exp\left[-\frac{\Delta S}{R}\right] \cdot \exp\left[\frac{\Delta H}{RT}\right] \tag{6}$$

where k_B is Boltzmann's constant, R is the gas constant; h is Planck's constant, ΔH the activation enthalpy and ΔS the activation entropy.

2.2.4. Thermostimulated currents.

TSC measurements were carried out with home-made equipment previously described [19]. Pellets ($\phi = 0.8\,cm$) were inserted between two plate steel electrodes. The sample cell was filled with dry helium. For recording complex thermograms, the sample was polarized by an electrostatic field $E_p = 1.2\,kV\,mm^{-1}$ during $t_p = 2\,min$ over a temperature range from the polarization temperature T_p down to the freezing temperature T_0. Then the field was turned off and the depolarization current was recorded with a constant heating rate ($q_h = +7\,°C\,min^{-1}$), the equivalent frequency of the TSC spectrum was $f_{eq} \sim 10^{-2}$–$10^{-3}\,Hz$. Elementary TSC thermograms were obtained with a poling window of $5\,°C$. Then the field was removed and the sample cooled down to a temperature $T_{cc} = T_p - 40\,°C$. The depolarization current was normalized to be homogeneous with dipolar conductivity σ and it was recorded with a constant heating rate q_h. The series of elementary thermograms was recorded by shifting the poling window by $5\,°C$ towards higher temperature.
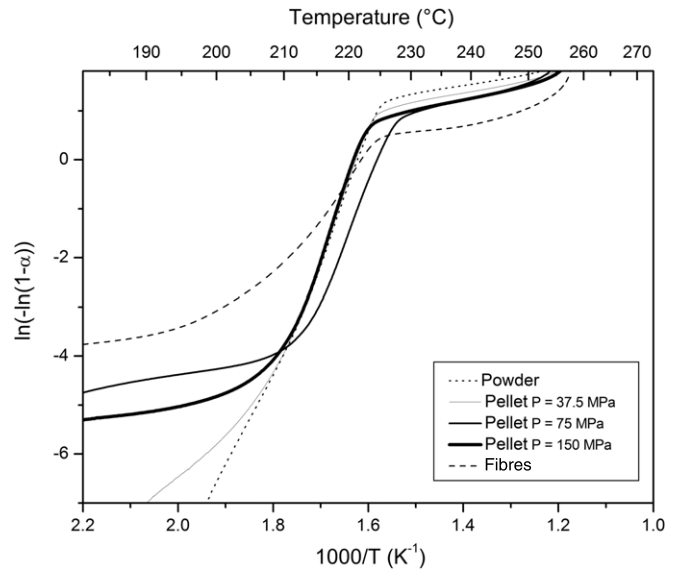
3. Results and discussion

3.1. Thermal stability

TGA experiments have been carried out in order to define the stability and the influence of sampling (powder or pellet). Figure 1 shows two thermograms of powder and pellet,
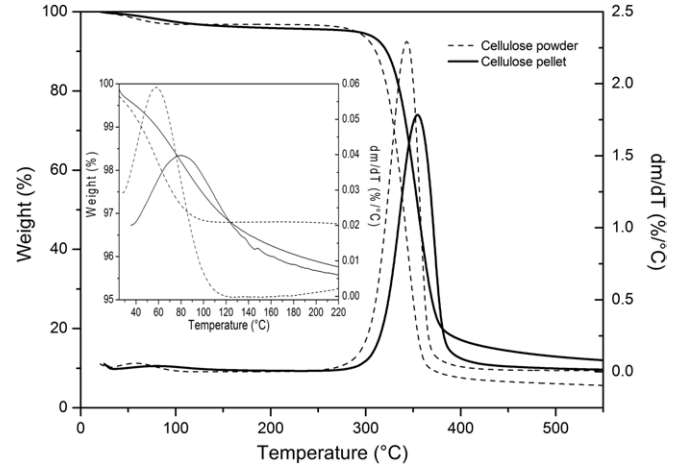
Figure 1. Thermogravimetry thermograms for cellulose powder and pellet, from room temperature to $550\,°C$ at $10\,°C\,min^{-1}$.


Figure 2. Broido's representation for different samples of cellulose.

respectively. For powder, two weight losses are observed, i.e. 60 and $343\,°C$. The first one is associated with water according to infra-red spectrometer and the second one with the cellulose degradation. These two events are consistent with the literature [4, 5, 11–13, 38–40]. For pellets, a slight shift of these two weight losses towards higher temperatures is observed, i.e. 82 and $355\,°C$. This shift is probably due to the increase in hydrogen bond interactions associated with the decrease in length between hydrophilic groups.

The Broido method [35] has been used to determine activation energy of degradation. Results are shown in figure 2 and reported in table 1. Three samplings of cellulose (i.e. powder, pellet and fibres) and three pressures are analysed. The activation energy of pellets, near $238\,kJ\,mol^{-1}$, is higher than powder and fibres. This value is consistent with Varhegyi and Jakab's data [41]. In the case of pellets, we do not observe influence of pressure on this physical parameter. Analogous behaviour has been found in tablets of microcrystalline cellulose [42]. Consequently, pellets can be used for dielectric

Table 1. Activation energy of degradation for different cellulose samples.

Cellulose	Powder	Pellet ($P = 37.5\,\mathrm{MPa}$)	Pellet ($P = 75\,\mathrm{MPa}$)	Pellet ($P = 150\,\mathrm{MPa}$)	Fibres
E_a (kJ mol^{-1})	225 ± 4	232 ± 4	237 ± 13	238 ± 10	120 ± 3
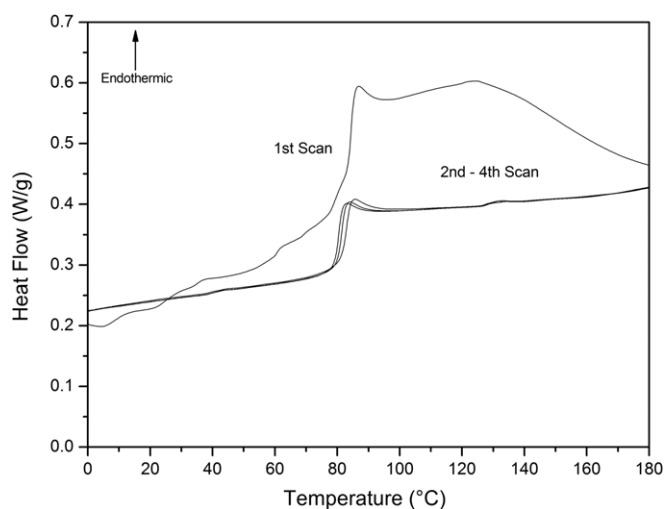
Figure 3. Heat flow thermograms of cellulose pellets for four successive scans from 0 to $180\,°\mathrm{C}$ at $20\,°\mathrm{C\,min^{-1}}$.

analysis. The stability temperature range as defined by TGA reaches $200\,°\mathrm{C}$.

3.2. Thermal transitions

DSC thermograms of cellulose are reported in figure 3. Four consecutive heating cycles have been carried out to obtain a repeatable result in dehydrated cellulose. A large endothermic peak associated with water loss during the heating [11, 43] is observed for the first thermogram. For the following thermograms the heat capacity step characteristic of the glass transition is pointed out. The T_g of dehydrated cellulose is found at $84 \pm 1\,°\mathrm{C}$ with a $\Delta C_p = 0.30 \pm 0.01\,\mathrm{J\,g^{-1}\,°C^{-1}}$. The ΔC_p value is comparable to the values measured for synthetic polymers [44].

Figure 4 reports an endothermic peak superimposed to T_g appearing when the sample was heated at $60\,°\mathrm{C}$ for different durations from 15 min to 3 h. This weak phenomenon is reversible so that it looks like physical ageing [45, 46]. Its kinetics must be fast since it is independent from annealing time in contrast to usual physical ageing. It is interesting to report here that physical ageing has been observed by TSC in amorphous ethyl cellulose [47]. At this stage, the phenomenon observed in cellulose may be attributed to the disruption of hydrogen bonds in the amorphous phase.

Figure 5 shows heat flow measurements of cellulose with water content from 0% to 5%. The glass transition is strongly dependent upon hydration. T_g and ΔC_p of cellulose decrease when the hydration level increases. A strong plasticization effect is observed and confirms previous results [11, 16, 18].

The properties of biopolymers are dependent on their hydration due to hydrophilic groups [18]. Authors differentiate three kinds of water in biopolymers: free water, freezing-bound water and non-freezing bound water [11, 42, 48, 49].
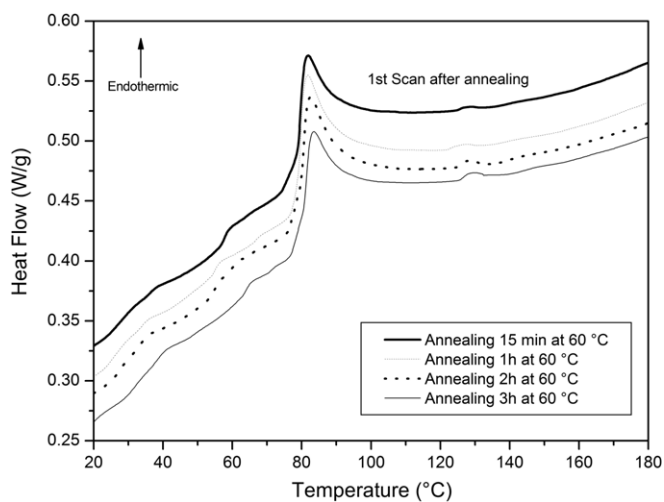
Figure 4. DSC thermograms of cellulose after different annealing times from 20 to $180\,°\mathrm{C}$ at $20\,°\mathrm{C\,min^{-1}}$.
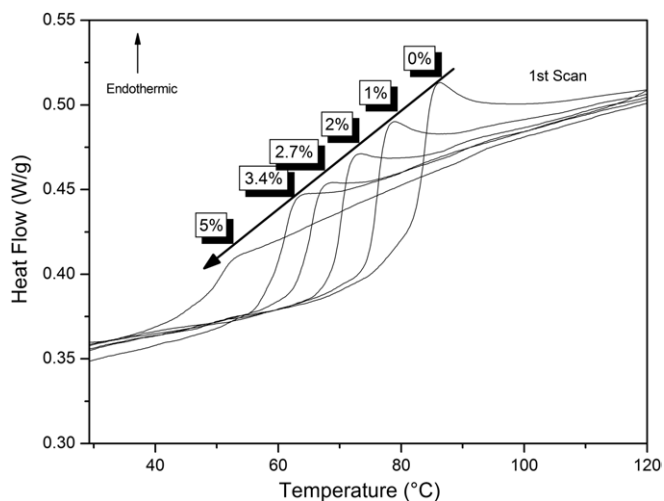
Figure 5. DSC thermograms of hydrated cellulose from 30 to $120\,°\mathrm{C}$, recorded at $20\,°\mathrm{C\,min^{-1}}$. The hydration level h is indicated for each thermogram.

This classical thermal analysis reveals that water interacts with the polymer; i.e. free water is dismissed. The following dielectric analysis allows us to shed some light on this behaviour.

3.3. Isothermal dynamic dielectric response

The complex dielectric permittivity is explored by DDS. In order to investigate the water influence on the dielectric response, experiments are carried out with different hydration levels. Figure 6 shows the relaxation map of 7% hydration cellulose. These three-dimensional diagrams point out four dielectric events: at low temperature two broad secondary relaxation modes called γ and β, at
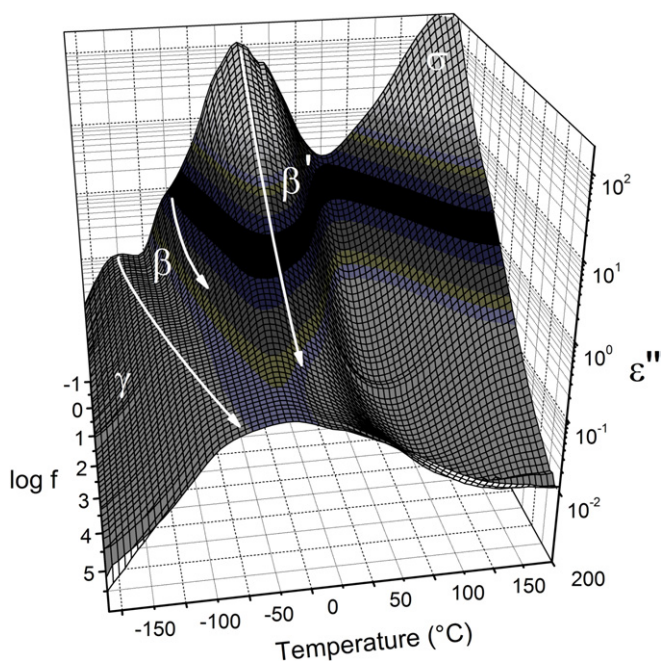
Figure 6. Imaginary part of dielectric permittivity versus temperature (-160 to $200\,^\circ$C) and frequency (10^{-1} to 10^6 Hz), for cellulose pellets with 7% water content.

(This figure is in colour only in the electronic version)
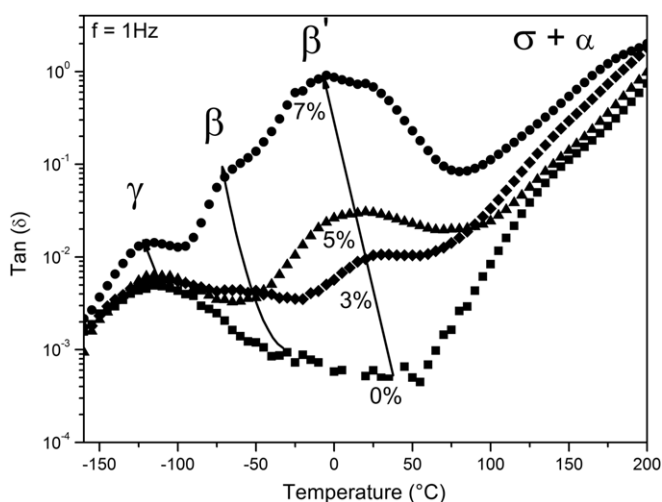
Figure 7. Tan (δ) dielectric loss factor versus temperature (-160 to $200\,^\circ$C) at 1 Hz for cellulose at different hydration levels.

higher temperature a wide quasi-isothermal relaxation and conductivity phenomenon labelled β' and σ respectively. The α relaxation mode associated with the dielectric manifestation of glass transition is hidden by this conduction phenomenon. The σ electrical conduction manifestation has been already associated with charge transport [26] or the Maxwell–Wagner–Sillars effect [28].

The tan (δ) loss factor of cellulose with different water contents; i.e. 0% to 7% is shown in figure 7. In the low temperature region, γ relaxation mode is pointed out for each hydration level in contrast to β relaxation mode which is only visible for 3% and 7%. In consequence for 5% water contents and near $-50\,^\circ$C, the tan (δ) loss factor curve is below 3%. At
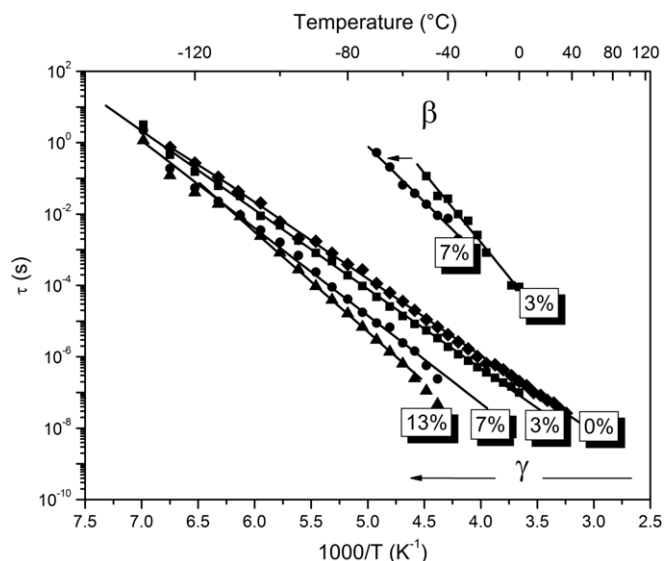
Figure 8. Arrhenius diagram of the low temperature relaxation modes (γ and β) obtained by DDS for cellulose at different water contents.

higher temperatures ($>80\,^\circ$C) a similar behaviour is observed due to the influence of α relaxation mode hidden by conduction phenomenon. From -50 to $80\,^\circ$C the additional dielectric contribution labelled β' appears for hydrated samples. This peak is also observed on the three-dimensional map of ε'' (figure 6). The strength of this mode increases with the hydration level. Such a β' relaxation mode has been already reported in the literature [42, 50, 51] and it has been associated with conformational changes of confined water. Banys *et al* [50] confirm this molecular origin in porous materials.

The relaxation times τ have been extracted from dielectric data and reported in the Arrhenius diagram of figure 8. The relaxation times of the two secondary relaxation modes are well fitted by an Arrhenius law but their behaviour is dependent upon hydration level. For the γ mode, the series of relaxation times corresponding to various hydration levels converges at low temperature and follows an 'anti-compensation' law:

$$\tau(T) = \tau_c \cdot \exp\left[\frac{\Delta H}{R}\left(\frac{1}{T} - \frac{1}{T_c}\right)\right] \qquad (7)$$

where $T_c = -130\,^\circ$C and $\tau_c = 2.4$ s are the temperature and the time of the convergence point, respectively. This τ_c value is quite high for a low temperatures relaxation. As a comparison, it is near τ_c value of the lignin main relaxation [52].

It is interesting to note the value of $\Delta H = 40\,$kJ mol^{-1} is comparable to the one of hydrogen bond. The activation parameters are reported in figures 9 and 10. These results are coherent with published data from mechanical and dielectric studies [28–31, 51]. The activation energy of the γ mode increases with the hydration level whereas it decreases for the β mode. The increase in the activation energy indicates the decrease in its molecular mobility [23, 28, 53]. The hydroxyl and hydroxymethyl groups form water–polymer complexes. Hydrogen bonds decrease the water–polymer complex mobility. Hydration plays the role of an anti-plasticizer for the γ mode. The decrease in the activation
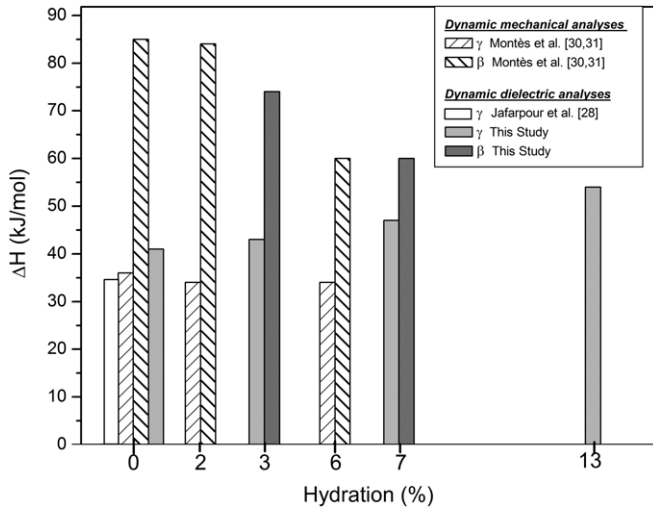
Figure 9. Activation energy of γ and β mechanical and dielectric relaxation modes for different moisture contents for cellulose.
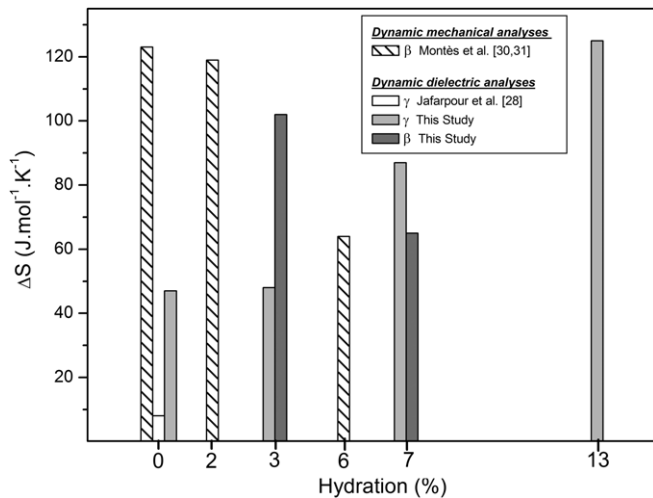

Figure 10. Activation entropy of γ and β mechanical and dielectric relaxation modes for different moisture contents for cellulose.

energy with hydration for the β mode indicates that its molecular mobility increases. The water molecules interfere with existing hydrogen bonds, increasing the free volume between the polymer chains and reducing the hindrance for the local chain mobility. Hydration plays the role of a plasticizer for the β mode. It can be involved in the same behaviour for the β mode of epoxy assemblies associated with hydroxyether entities. Chevalier *et al* [54] also observe the low temperature convergence point and the decrease in the activation energy with the increase in hydration level due to hydrothermal ageing. The evolution of mobility is linked with the physical environment modification. These dynamic dielectric data have been completed towards lower frequencies by thermostimulated current experiments.

3.4. Correlation with non-isothermal dielectric response

The normalized depolarization current σ is plotted versus temperature in figure 11, for different water contents. In the low temperature range and for 0% hydration two relaxation modes are observed. The γ relaxation mode assigned to
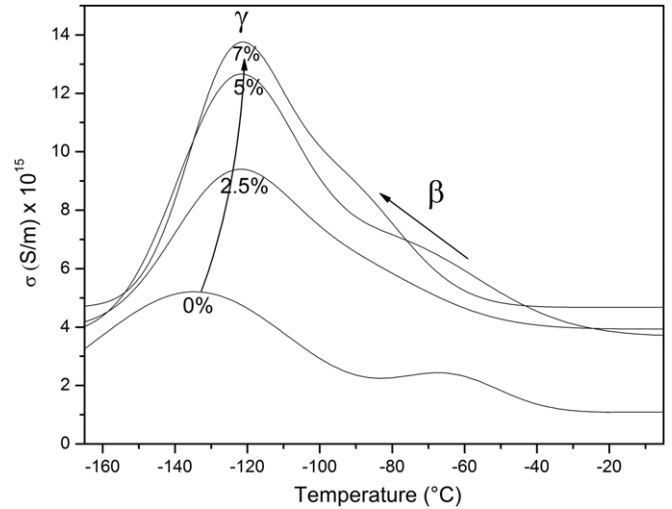

Figure 11. Complex TSC thermogram of cellulose at four states of hydration from -160 to $-10\,^{\circ}$C at $7\,^{\circ}$C min^{-1}.
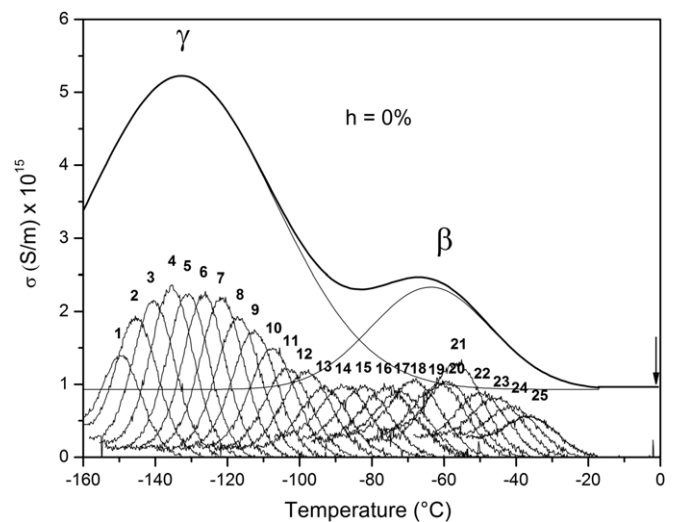
**Figure 12.** Complex TSC thermogram with their associated elementary thermograms for γ and β relaxation modes ($-160\,^{\circ}$C to $0\,^{\circ}$C at $7\,^{\circ}$C min^{-1}) for cellulose in the dehydrated state.

the side groups' reorientation is located at $-135\,^{\circ}$C. The β relaxation mode attributed to localized movements of short sequences of the main chain of cellulose is pointed out at $-65\,^{\circ}$C. In contrast to the β relaxation mode, the maximum of the γ relaxation mode increases with the hydration level from $-135\,^{\circ}$C at 0% to $-120\,^{\circ}$C at 7%. We observe a merging of these two relaxation modes upon increasing hydration level. These results are coherent with SDD; i.e. hydration plays the role of an anti-plasticizer for the γ mode and a plasticizer for the β mode. The anti-plasticization phenomenon due to hydration is also observed in micromechanical spectroscopy as shown by Lamure *et al* from studies of the main retardation mode associated with glass transition of proteoglycan subunits [55]. Fractional polarizations allow us to extract activation parameters for different hydration states. A series of elementary thermograms is obtained and reported in figure 12 for 0% hydration.

Results of the two dielectric methods are reported for each hydration state. The β DDS relaxation mode is detectable
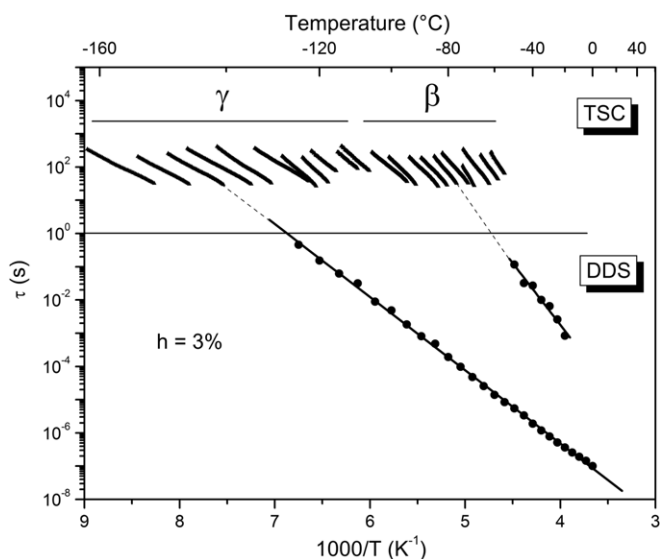
Figure 13. Arrhenius diagram from combined DDS and TSC in the low temperature range ($T < 0\,°C$) for 3% hydrated cellulose.
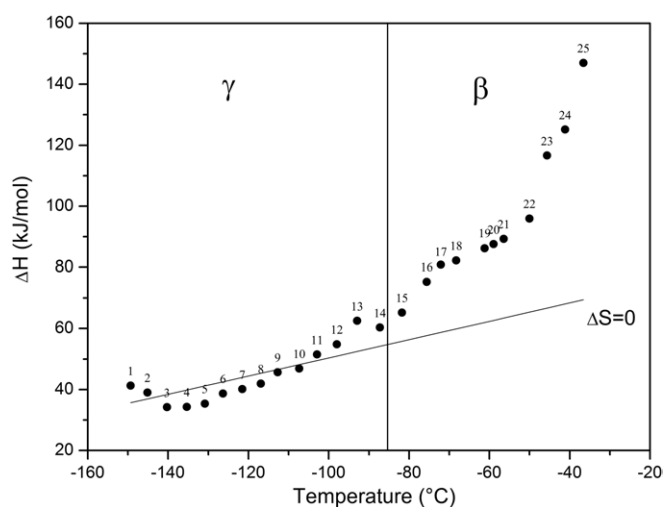
Figure 14. Activation enthalpy versus temperature for the elementary thermograms constituting the low temperature relaxation modes in dehydrated cellulose.

for 3% and 7% hydration level only. According to Montès *et al* [30, 31, 56], the β relaxation mode has been associated with cellulose moisture content; it is not always detectable by DDS. In figure 13, Arrhenius diagram of DDS and TSC data is shown for 3% of water. The relaxation times obtained by DDS are extrapolated until TSC data; a good correlation is performed. The correlation between γ and β modes in DDS and TSC allows us to confirm the molecular origin of these two modes. Then, the β mode can be followed for each state of hydration by TSC.

The activation enthalpy versus temperature for γ and β relaxation modes is reported in figure 14 with the Starkweather line [57] associated with the null activation entropy. The experimental points related to the γ mode lie close to the Starkweather line indicating that the localized mobility of the side groups is not cooperative. In contrast, activation enthalpies of the β mode depart from the null activation entropy
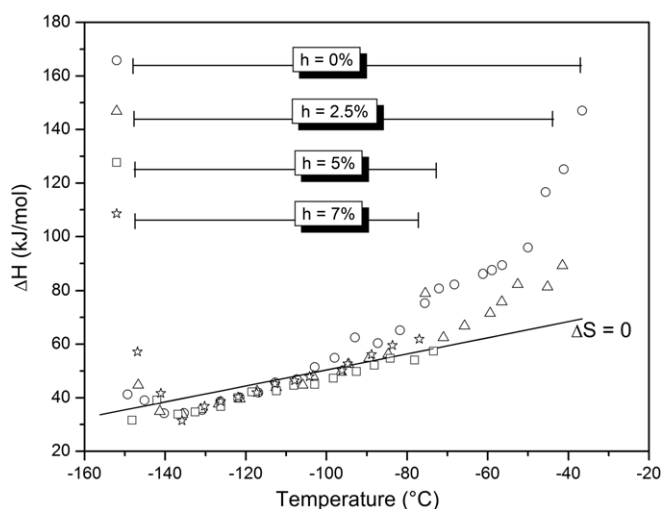
Figure 15. Activation enthalpy versus temperature for the elementary thermograms constituting the low temperature relaxation modes for cellulose at four states of hydration.

line reflecting a cooperative mobility of the β_{1-4} glycosidic bonds of cellulose.

The influence of hydration level on the activation enthalpies versus temperature for the elementary process of γ and β relaxation modes is reported in figure 15. The enthalpy range and ΔH_{max} values decrease when the hydration level increases. The cooperative behaviour of the β relaxation is strongly dependent upon hydration. For water contents between 0% and 2.5%, the β relaxation is characterized by a cooperative behaviour; otherwise for hydration level between 2.5% and 7%, a non-cooperative behaviour is exhibited. This evolution has been assigned to an increase in the hydrogen bond density leading to a more localized cooperative mobility.

4. Conclusion

The combination of both thermal analyses and dielectric spectroscopy has been applied to a thorough investigation of the molecular dynamics in hydrated cellulose.

The thermal stability of the polymer and the initial water content is assessed using TGA. Thermal behaviour of cellulose is dependent on the morphology of the samples. The activation energy of degradation for pellets is higher than for the other forms (fibres, powder). In contrast, pressure does not affect the degradation behaviour of pellets.

Original data have been extracted from DSC showing the influence of water on the viscoelastic behaviour of cellulose through the analysis of the dependence upon hydration of the glass transition temperature T_g. At the molecular scale, bound water is hydrogen bonded to polar sites of cellulose macromolecules. At the macroscopic scale, water molecules play the role of a plasticizer for cellulose lowering its T_g.

DDS combined with TSC has allowed us to follow more localized molecular mobility occurring in the glassy state as a function of hydration. According to the literature, the origin of the β relaxation mode is localized movements of the β_{1-4} glycosidic bonds of cellulose. This mode is characterized by activation entropies that vanish for higher water contents

indicating a localization of the molecular mobility. It is plasticized by water like the glass transition. This analogy is explained by a common origin of both mechanisms: the mobility of the cellulose backbone. In fact, they differentiate only by the scale of the mobile units.

From previous works, the γ relaxation mode has been attributed to the molecular mobility of the side groups of glycosidic rings. The behaviour of this γ mode upon hydration is opposite to the previous ones. The series of relaxation times corresponding to various hydration levels follows an anti-compensation law with an activation enthalpy comparable to the one of hydrogen bond. Water acts as an anti-plasticizer in a hydrogen bonded network involving $-CH_2OH$ and $-OH$ groups with water molecules. It is interesting to note here that such an arrangement is common to biopolymers containing glycosidic rings.

References

[1] Seguin B 2003 *C. R. Geosci.* **335** 569–75
[2] Wegener G and Fengel D 1984 *Wood: Chemistry Ultrastructure Reactions* (Berlin: de Gruyter & Co)
[3] Gani A and Naruse I 2007 *Renew. Energy* **32** 649–61
[4] Hanakoa T, Inoue S, Uno S, Ogi T and Minowa T 2005 *Biomass Bioenergy* **28** 69–76
[5] Kaloustian J, El-Moselhy T F and Portugal H 2003 *Thermochim. Acta* **401** 77–86
[6] Barbosa M A, Granja P L, Barrias C C and Amaral I F 2005 *ITBM-RBM* **26** 212–17
[7] Wang Z H, Chien W C, Yue T W and Tang S H 2008 *J. Membr. Sci.* **310** 141–8
[8] Galop M, Lamure A and Lacabanne C 2000 *J. Appl. Polym. Sci.* **78** 8–13
[9] Boudet A, Kajita S, Grima-Pettinati J and Goffner D 2003 *Trends Plant Sci.* **8** 576–81
[10] Shlensky O F and Vaynshteyn E F 1989 *J. Therm. Anal.* **35** 1477–82
[11] Szczesniak L and Rachocki A 2007 *Cellulose* **15** 445–51
[12] Devallencourt C, Saiter J M and Capitaine D 1996 *Polym. Degradation Stab.* **52** 327–34
[13] Devallencourt C, Saiter J M and Capitaine D 1999 *Polym. Eng. Sci.* **39** 413–21
[14] Agrawal R K 1988 *Can. J. Chem. Eng.* **66** 403–12
[15] Shafizadeh F 1968 *Adv. Carbohydrate Chem.* **23** 419–74
[16] Batzer H and Kreibich U T 1981 *Polym. Bull.* **5** 585–90
[17] Vittadini E, Dickinson L C and Chinachoti P 2001 *Carbohydrate Polym.* **46** 49–57
[18] Salmèn N L and Back E L 1977 *Tappi* **60** 137–40
[19] Teyssèdre G and Lacabanne C 1996 *Techniques De L'Ingénieur Traité Analyse Et Caractérisation* P3770 pp 1–7
[20] Hatakeyama T 1989 Structure and properties of the amorphous region of cellulose *Cellulose Structural And Functional Aspects* ed J F Kennedy *et al* (Chichester: Halsted Press/ Wiley) pp 46–52
[21] Yu L and Christie G 2001 *Carbohydrate Polym.* **46** 179–84
[22] Einfeldt J, Meißner D and Kwasniewski A 2000 *Macromol. Chem. Phys.* **201** 1969–75
[23] Einfeldt J, Meißner D, Kwasniewski A, Gruber E and Henricks R 2000 *Macromol. Mater. Eng.* **283** 7–14
[24] Meißner D, Einfeldt J and Kwasniewski A 2000 *J. Non-Crystal. Solids* **275** 199–209
[25] Einfeldt J, Meißner D and Kwasniewski A 2001 *Prog. Polym. Sci.* **26** 1419–72
[26] Einfeldt J, Meißner D and Kwasniewski A 2003 *J. Non-Cryst. Solids* **320** 40–55
[27] Einfeldt J, Meißner D and Kwasniewski A 2004 *Cellulose* **11** 137–50
[28] Jafarpour G, Dantras E, Boudet A and Lacabanne C 2007 *J. Non-Cryst. Solids* **353** 4108–15
[29] Jafarpour G, Roig F, Dantras E, Boudet A and Lacabanne C 2009 *J. Non-Cryst. Solids* **355** 1669–72
[30] Montès H, Mazeau K and Cavaillé J Y 1997 *Macromolecules* **30** 6977–84
[31] Montès H, Mazeau K and Cavaillé J Y 1998 *J. Non-Cryst. Solids* **235–237** 416–21
[32] Kent M and Meyer W 1983 *J. Phys. D: Appl. Phys.* **16** 915–25
[33] Sugimoto H, Miki T, Kanayama K and Norimoto M 2008 *J. Non-Cryst. Solids* **354** 3220–24
[34] Švedas V 1998 *J. Phys. D: Appl. Phys.* **31** 1752–6
[35] Broido A 1969 *J. Polym. Sci.* A-2 **7** 1761–73
[36] Peng L, Long Y, Hongsheng L, Ling C and Lin L 2009 *Carbohydrate Polym.* **77** 250–3
[37] Havriliak S and Negami S 1966 *J. Polym. Sci.* C **14** 99–117
[38] Kifani-Sahban F, Belkbir L and Zoulalian A 1996 *Thermochim. Acta* **284** 341–9
[39] Franceschi E, Luciano G, Carosi F, Cornara L and Montanari C 2004 *Thermochim. Acta* **418** 39–45
[40] Sun J X, Sun X F, Zhao H and Sun R C 2004 *Polym. Degradation Stab.* **84** 331–9
[41] Varhegyi G and Jakab E 1994 *Energy Fuels* **8** 1345–52
[42] Nilsson M, Alderborn G, and Strømme M 2003 *Chem. Phys.* **295** 159–65
[43] Ford J L 1999 *Int. J. Pharm.* **179** 209–28
[44] Wunderlich B 2005 *Thermal Analysis Of Polymeric Materials* (Berlin: Springer)
[45] Struik L C E 1978 *Physical Aging in Amorphous Polymers and Other Materials* (Amsterdam: Elsevier)
[46] Samouillan V, André C, Dandurand J and Lacabanne C 2004 *Biomacromolecules* **5** 958–64
[47] Diogo H P and Moura-Ramos J J 2009 *J. Polym. Sci.* B **47** 820–9
[48] Nakamura K, Hatakeyama T and Hatakeyama H 1981 *Textile Res. J.* **51** 607–13
[49] Hatakeyama H and Hatakeyama T 1998 *Thermochim. Acta* **308** 3–22
[50] Banys J, Kinka M, Macutkevič J, Voelkel G, Boehlmann W, Umamaheswari V, Hartmann M and Poeppl A 2005 *J. Phys.: Condens. Matter* **17** 2843–57
[51] Einfeldt J and Kwasniewski A 2002 *Cellulose* **9** 225–38
[52] Jafarpour G, Dantras E, Boudet A and Lacabanne C 2008 *J. Non-Cryst. Solids* **354** 3207–14
[53] Henry F, Costa L C and Devassine M 2005 *Eur. Polym. J.* **41** 2122–26
[54] Chevalier M, Dantras E, Tonon C, Guigue P, Lacabanne C, Puig C and Durin C 2010 *J. Appl. Polym. Sci.* **115** 1208–14
[55] Lamure A, Harmand M F and Lacabanne C 1990 *J. Biomed. Mater. Res.* **24** 735–47
[56] Montès H and Cavaillé J Y 1999 *Polymer* **40** 2649–57
[57] Starkweather H W 1981 *Macromolecules* **14** 1277–81